Hindawi
Journal of Spectroscopy
Volume 2020, Article ID 2725186, 9 pages
https://doi.org/10.1155/2020/2725186

*Research Article*

# Change Detection in Multitemporal High Spatial Resolution Remote-Sensing Images Based on Saliency Detection and Spatial Intuitionistic Fuzzy C-Means Clustering

**Liang Huang**,[1,2] **Qiuzhi Peng**,[1,2] **and Xueqin Yu**[3]

[1]*Faculty of Land Resource Engineering, Kunming University of Science and Technology, Kunming 650093, China*
[2]*Surveying and Mapping Geo-Informatics Technology Research Center on Plateau Mountains of Yunnan Higher Education, Kunming 650093, China*
[3]*Kunming Surveying and Mapping Institute, Kunming 650051, China*

Correspondence should be addressed to Liang Huang; kmhuangliang@163.com

Received 13 November 2019; Revised 22 February 2020; Accepted 2 March 2020; Published 23 March 2020

Academic Editor: Vincenza Crupi



In order to improve the change detection accuracy of multitemporal high spatial resolution remote-sensing (HSRRS) images, a change detection method of multitemporal remote-sensing images based on saliency detection and spatial intuitionistic fuzzy C-means (SIFCM) clustering is proposed. Firstly, the cluster-based saliency cue method is used to obtain the saliency maps of two temporal remote-sensing images; then, the saliency difference is obtained by subtracting the saliency maps of two temporal remote-sensing images; finally, the SIFCM clustering algorithm is used to classify the saliency difference image to obtain the change regions and unchange regions. Two data sets of multitemporal high spatial resolution remote-sensing images are selected as the experimental data. The detection accuracy of the proposed method is 96.17% and 97.89%. The results show that the proposed method is a feasible and better performance multitemporal remote-sensing image change detection method.

## 1. Introduction

Remote-sensing image change detection is the main mean to identify and monitor the information on land-covered change caused by human activities and natural processes. At present, change detection has been widely used in forest cover monitoring [1, 2], land use/land cover monitoring [3, 4], disaster assessment [5], urban expansion analysis [6, 7], and other fields.

In general, remote-sensing image change detection methods can be divided into the direct comparison method and the postclassification comparison method. The direct comparison method is widely used in practice because of its simplicity and easy implementation [8]. The main steps of the direct comparison method include difference image construction, binary classification, analysis, and evaluation of detection results. At present, algebraic operation and image transformation methods are mainly used to obtain the difference image. The algebraic operation methods include univariate image differencing (UID) [9], vegetation index differencing (VID) [9], image rationing/log rationing (IR/LR) [9, 10], mixed method [11, 12], regression [9], and change vector analysis (CVA) [9]. These methods are widely used in multitemporal remote-sensing image change detection. For example, Huang et al. got the difference image of two temporal remote-sensing images by UID, IR, and mixed method, and then the 2D-OTSU method improved by the firefly algorithm was used to segment the difference image to obtain the change areas [13]; in order to solve the impact of speckle noise on the change detection accuracy of multitemporal SAR images, Gao et al. proposed a modified-log-ratio (MLR) operator for change detection of targets in forest concealment [14]. Nordberg and Evertson used VID combined with the image regression method to study the impact on decrease of vegetation coverage in the Swedish mountains caused by increased mining [15]. Gong et al. proposed a

change detection method for multispectral imagery based on the generative discriminatory classified network (GDCN): the CVA and OTSU methods were first used in the method to obtain the initial change detection result, and then the GDCN was used to obtain the final change detection result [16]. CVA is the most widely used method for the change detection of multitemporal optical remote-sensing images [17, 18], and some new methods have evolved into the basis of CVA, such as polar CVA (PCVA) [17], compressed CVA ($C^2VA$) [19], robust CVA (RCVA) [20, 21], and object-oriented CVA (OCVA) [22]. With the continuous enhancement of commercial HSRRS image acquisition ability, the HSRRS image has gradually become the main data source of change detection. However, with the improvement of spatial resolution, the details of the ground objects become more and more abundant, and the spectral heterogeneity is also increasing. So, the method of constructing the difference image based on pixel-by-pixel comparison faces great challenges [16]. In the method of direct object comparison, it is very difficult to acquire an image object effectively in HSRRS image change detection. The methods of binary classification for different images mainly include clustering [23, 24], threshold segmentation [13], Bayesian [25], support vector machine (SVM) [26], and CRF [27]. Among them, clustering is an effective method for unsupervised binary classification of different images. For example, Atasever proposed an unsupervised change detection method based on reconstruction independent component analysis and ABC-K-means clustering: four different functions were first used to achieve difference images, then four different matrices were projected to one feature of reconstruction independent component analysis, and clustering was performed; finally, K-means tuned by artificial bee colony (ABC-K-means) clustering technique has been developed and proposed by following a different strategy in the clustering phase [24]. Ghosh used fuzzy C-means (FCM) and Gustafson Kessel clustering (GKC) to analyze the difference image obtained by CVA and got the change results [28]. Gong et al. obtained the difference image by fusion of the mean ration image and log ration image, and then fuzzy local information C-means (FLICM) was applied to the difference image to obtain the change area [11]. However, there are some problems with the clustering algorithm represented by traditional FCM, such as the objective function is easy to fall into local minimum, the function convergence speed is slow, and it is sensitive to initial value and noise, which affects the accuracy of change detection.

In recent years, with the development of saliency detection technology, it has been widely used in image segmentation, target recognition, image retrieval, and other fields [29]. Now, saliency detection is also used in change detection. For example, aiming at the complex statistical distributions of the change features, Hou et al. proposed the semisupervised building change detection method based on saliency detection combined with the morphological building index (MBI) [30]. Guo and Zhang first got the fused difference image and feature difference image, then cosaliency strategy was used to obtain the saliency maps of two difference images, and FLICM was finally used to cluster and fuse the saliency maps to achieve the final change detection results [31]. The existing change detection methods based on saliency detection mainly rely on the strategy of obtaining the difference image first and then saliency detection. This strategy is based on the difference image to perform saliency detection to obtain the change areas, so the quality of the difference image directly affects the accuracy of subsequent change detection. The high spatial resolution remote-sensing image has the problems of "the same object with different spectra" and "different objects with the same spectrum." Because the spatial features of the image are ignored, the high resolution remote-sensing image obtained by IR, UID, and CVA methods has poor quality of the difference image. In order to solve this problem, this paper combines the advantages of the saliency detection method of image segmentation, proposes a hypothesis: if there are no changes in the two temporal images, the saliency maps should be roughly the same, and if they are different, it should be that the surface has changed and experiments should be designed to verify it. The saliency detection method based on clustering is used in this paper [32]. This method comprehensively considers the spatial cues and contrast cues for the image of the saliency detection and has better performance than the method that only considers the spectral features. So, a novel change detection method of multitemporal high spatial resolution remote-sensing images based on saliency detection and SIFCM clustering is proposed in this paper. We tried a strategy of the first saliency detection and then difference image acquisition in this method; here, the performance of saliency detection is fully utilized to improve the quality of the difference image. In view of the shortcomings of the traditional FCM, after obtaining the difference image, the SIFCM [33] clustering method is introduced to solve the problems of noise sensitivity and lack of spatial information in the difference image analysis. The rest of this paper is organized as follows. The details of the research method are introduced into Section 2, experimental results and analysis are shown in Section 3, and finally, conclusion is given in Section 4.

## 2. Research Method

We assume that $I^1$ and $I^2$ are remote-sensing images of the same region acquired in T1 and T2 different periods, and $I^1$ and $I^2$ are strictly registered. Firstly, the saliency detection method based on clustering is used to detect the saliency of $I^1$ and $I^2$, and the saliency maps $S_1$ and $S_2$ of $I^1$ and $I^2$ are obtained, respectively; then, the salience difference image (SDI) of $I^1$ and $I^2$ is obtained by subtraction of $S_1$ and $S_2$; next, the SIFCM clustering is performed to obtain change areas and nonchange areas of the SDI by binary classification; finally, a quantitative method is used to evaluate the accuracy of change detection results. The specific flow chart of the proposed method is shown in Figure 1.

*2.1. Construction of Saliency Difference Image.* If the remote-sensing images of the two periods do not change, the two images should have the same and similar saliency map. If

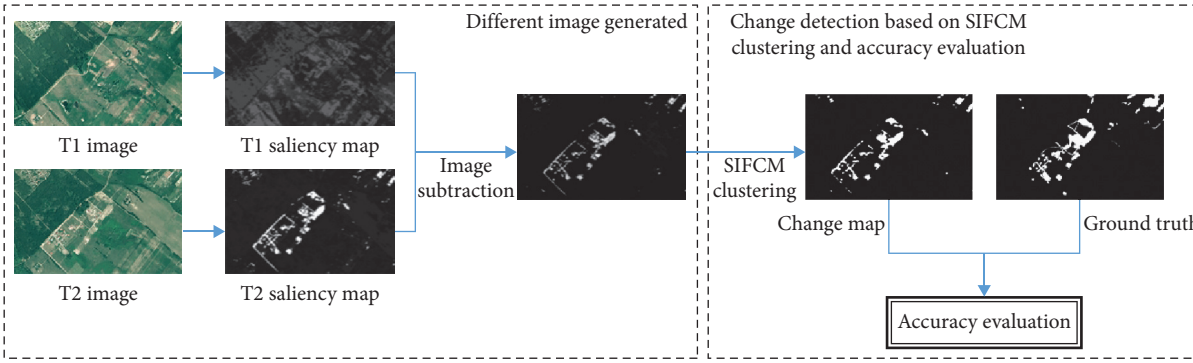


Figure 1: Flow chart of the proposed method.

there is a change in the remote-sensing images of two periods, the saliency map will also be different. Therefore, the saliency difference image can be obtained by the difference operation of the saliency maps of the two images; on this basis, the information of change and unchange in two temporal images is obtained. In order to get the saliency maps of two temporal remote-sensing images, the saliency detection method based on clustering is adopted in this paper [32], and its specific steps are as follows:

(1) The remote-sensing image $I^j$ is input.

(2) The $K$-means clustering method is used to divide $I^j$ into $K$-clusters.

(3) Formulas (1) and (2) are used to calculate the contrast cue $(\omega^c(k))$ and spatial cue $(\omega^s(k))$ of each cluster, respectively:

$$\omega^c(k) = \sum_{i=1, i\neq k}^{K} \left( \frac{n^i}{N} \left\| \mu^k - \mu^i \right\|_2 \right), \tag{1}$$

$$\omega^s(k) = \frac{1}{n^k} \sum_{j=1}^{M} \sum_{i=1}^{N_j} \left[ \Upsilon\left( \left\| z_i^j - o^j \right\|^2 \mid 0, \sigma^2 \right) \cdot \delta\left[ b\left( p_i^j \right) - C^k \right] \right]. \tag{2}$$

In formula (1), $\|\cdot\|_2$ is used to calculate the feature space; $n^i$ represents the number of pixels in the cluster $C^i$; $N$ means the number of pixels in the input image; and $\mu^k$ and $\mu^i$ are the cluster centers of $C^k$ and $C^i$.

In formula (2), $\delta(\cdot)$ is the Kronecker delta function; $o^j$ means the center of the input image $I^j$; Gaussian kernel $\Upsilon(\cdot)$ is used to calculate the Euclidean distance between the pixel $z_i^j$ and the image center $o^j$; variance $\sigma^2$ represents the normalized radius of the input image; the normalized coefficients $n^k$ means the pixel number of $C^k$; $p_i^j$ is the pixel $i$ in the input image $I^j$; $N_j$ represents the $j$ image lattice; $M$ is the number of input images; and $b(p_i^j)$ indicates the clustering index.

(4) Contrast cue and spatial cue are fused through the following formula.

$$p\left(C^k\right) = \prod_i \omega_i(k). \tag{3}$$

In formula (3), $\omega_i(k)$ represents the saliency clue.

(5) The final single image saliency map can be achieved by the following formula:

$$\text{saliency map} = S_j = p(x) = \sum_{k=1}^{K} p\left(x, C^k\right) = \sum_{k=1}^{K} p\left(x \mid C^k\right) p\left(C^k\right). \tag{4}$$

In formula (4), $x$ is the pixel in the input image.

The saliency maps ($S_1$ and $S_2$) of the two temporal remote-sensing images ($I^1$ and $I^2$) can be obtained through the saliency detection, and then formula (5) is used to gain the SDI by subtraction of the two temporal remote-sensing images of saliency maps:

$$\text{SDI} = 255 - \left| S_1 - S_2 \right|. \tag{5}$$

*2.2. Spatial Intuitionistic Fuzzy C-Means Clustering.* By using the SIFCM clustering method [33], the obtained SDI is classified into two classes: change class and nonchange class. The specific steps are as follows:

(1) $v_i (i = 1, \ldots, c)$ initial clustering centers are given, we set $c = 2$ in this paper.

(2) Membership $(u_{ij})$ is calculated by the following formula:

$$u_{ij} = \frac{1}{\sum_{k=1}^{2} \left( \left\| \left( x_j - v_i \right) / \left( x_j - v_k \right) \right\| \right)^{1/(m-1)}}. \tag{6}$$

In formula (6), $\|\cdot\|_2$ is used to calculate the Euclidean distance; $i = 1, 2$; $j = 1, \ldots, N$; $N$ is the number of pixels in the input image; $m$ is a constant, which is generally taken as 2; and $x_j$ means the pixel.

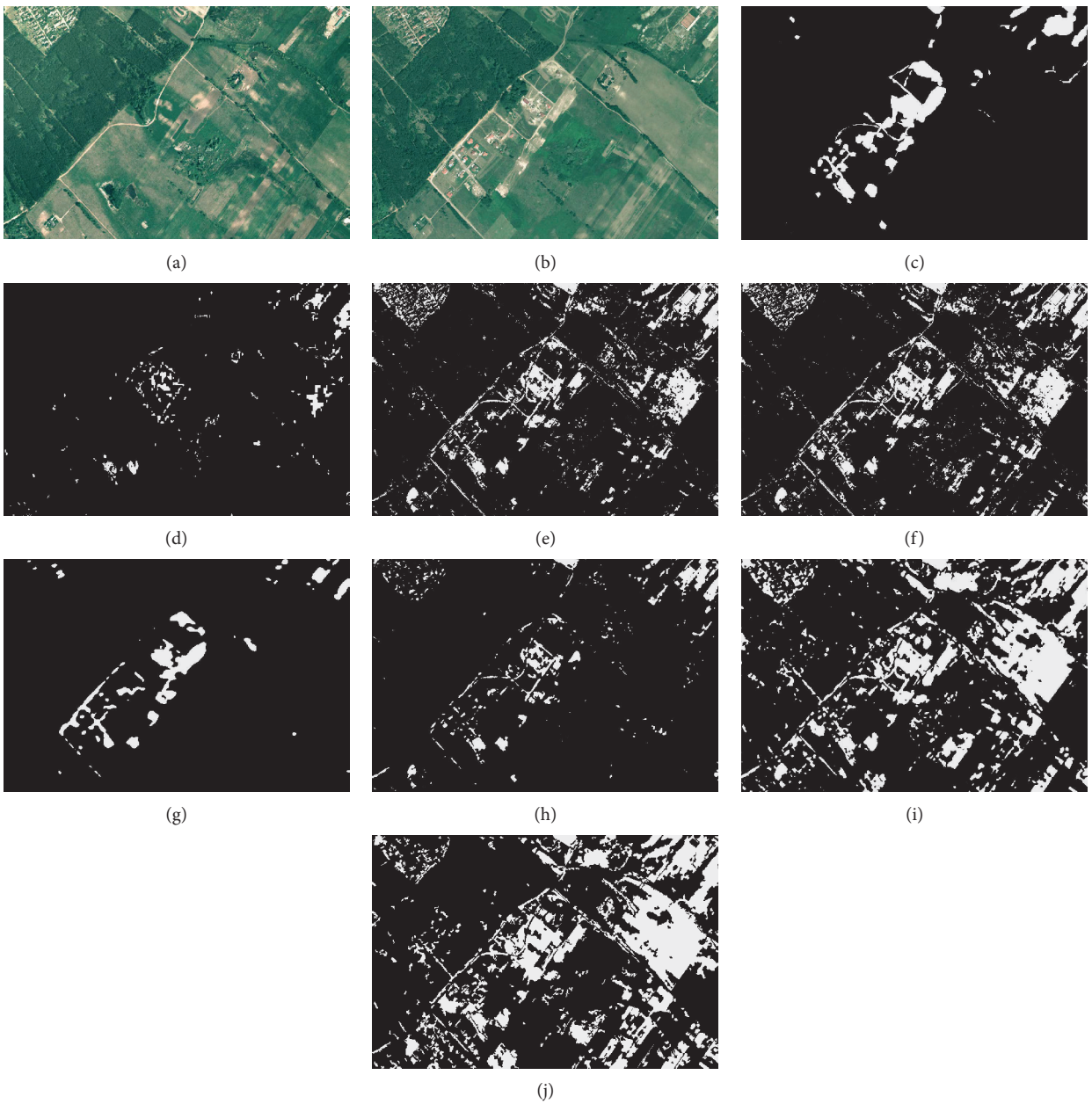


Figure 2: Visual comparison of change detection results in the first group of experiments. (a) Image 1. (b) Image 2. (c) Reference map. (d) IR-SIFCM. (e) UID-SIFCM. (f) CVA-SIFCM. (g) Proposed method. (h) PCA-K-means. (i) FLICM. (j) CWNN.

(3) The intuition index is calculated by the following formula:

$$\pi_{ij}(x) = 1 - u_{ij}(x) - \frac{\left(1 - u_{ij}(x)\right)}{\left(1 + \lambda . u_{ij}(x)\right)}. \tag{7}$$

In formula (7), $\lambda$ is the Lagrange multiplier.

(4) The new membership $(u'_{ij})$ is calculated:

$$u'_{ij} = u_{ij} + \pi_{ij}. \tag{8}$$

(5) Space function $(h_{ij})$ is computed:

$$h_{ij} = \sum_{k=\mathrm{NB}\left(x_j\right)} u_{ik}. \tag{9}$$

(i) In formula (9), $\mathrm{NB}(x_j)$ represents the neighborhood pixels of $x_j$, and $5 \times 5$ equal weight mask is used here.

(6) Membership $(u''_{ij})$ is updated by synthesizing spatial functions:

$$u''_{ij} = \frac{u'^{p}_{ij} h^{q}_{ij}}{\sum_{k=1}^{2} u'^{p}_{ij} h^{q}_{kj}}. \tag{10}$$

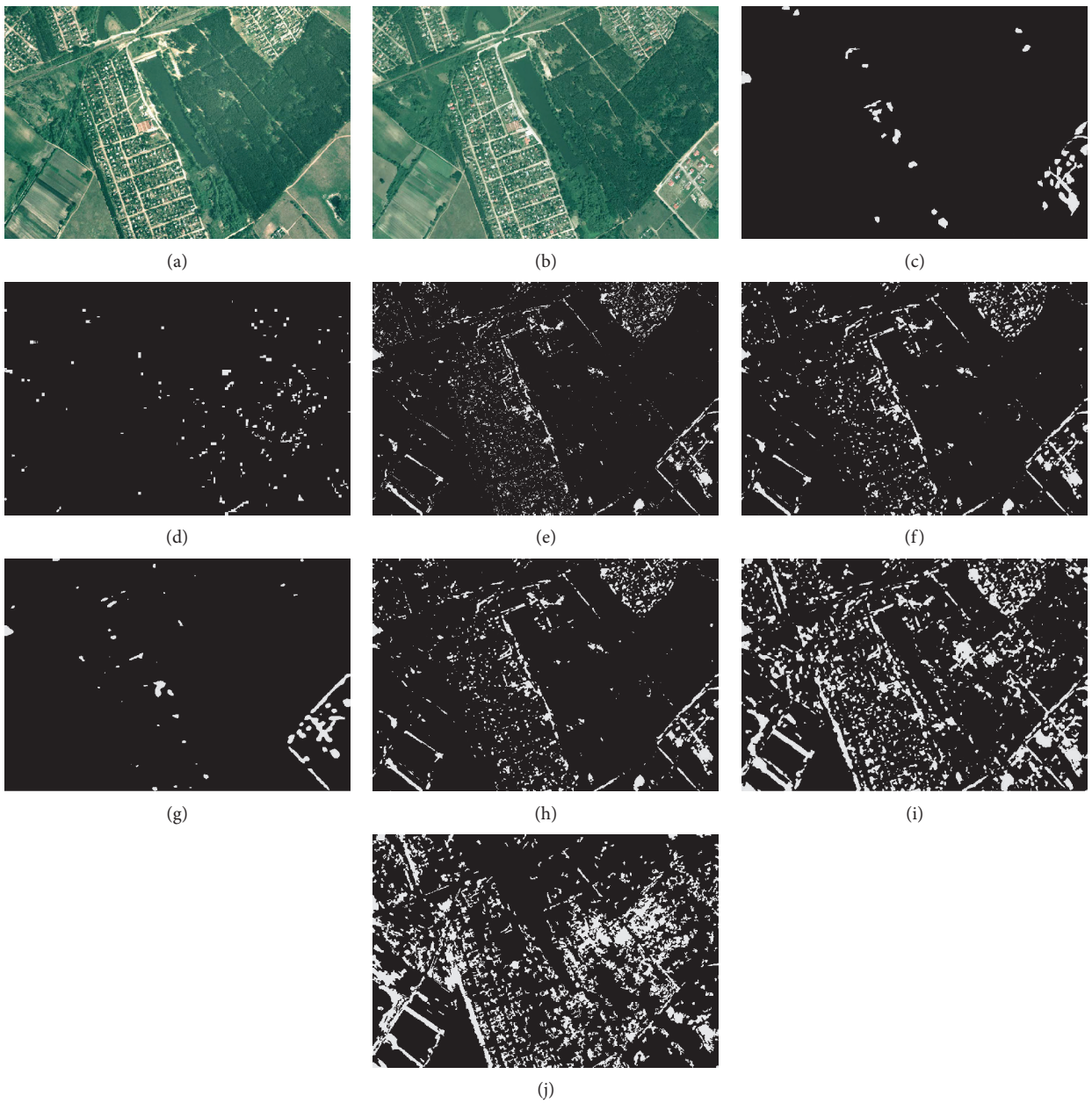


Figure 3: Visual comparison of change detection results in the second group of experiments. (a) Image 1. (b) Image 2. (c) Reference map. (d) IR-SIFCM. (e) UID-SIFCM. (f) CVA-SIFCM. (g) Proposed method. (h) PCA-K-means. (i) FLICM. (j) CWNN.

In formula (10), $p$ and $q$ determine the relative weights of initial membership and spatial function, respectively.

(7) The new cluster center is calculated according to the following formula:

$$v_i = \frac{\sum_{j=1}^{N} \left(u_{ij}''\right)^m x_j}{\sum_{j=1}^{N} \left(u_{ij}'\right)^m}. \tag{11}$$

(8) If $|u_{ij}^{\text{new}} - u_{ij}^{\text{prev}}| < \varepsilon$, where $\varepsilon$ equals to 0.05, the iterative operation is ended; otherwise, step 2 is returned. The maximum number of iterations (*max_iter*) is set as 50 in this paper.

## 3. Experimental Results and Analysis

*3.1. Experimental Data.* Two groups of multitemporal and high spatial resolution remote-sensing images are selected as the experimental data. Figures 2(a) and 2(b) show the first group of images, and Figures 3(a) and 3(b) show the second group of images. The two sets of data are all from SZTAKI air change benchmark set [34, 35], both of which are multitemporal aerial remote-sensing images, and the sizes of images are 952 pixels × 640 pixels. The images have three visible spectral bands: red, green, and blue, and image spatial resolution is 1.5 m. Figure 2(c) is the reference image of the first group, and Figure 3(c) is the reference image of the

second group. In Figures 2 and 3, the white area is the actual change area and the black area is the unchanged area.

The configuration of the experimental computer is Intel CORE i7-7700HQ, NVIDIA GTX 1060 6G GDDR5, and 8 GB DDR4; the SIFCM is implemented by tensorflow 2.0, and the saliency detection and difference images are implemented by Matlab 2018b.

*3.2. Comparative Experiment and Result Analysis.* In order to verify the effectiveness and reliability of the proposed method, two groups of comparative experiments were designed. UID, IR, CVA, and SDI proposed in this paper are used to construct difference images in the first group of experiments, and then SIFCM clustering is adopted to analyze the acquired difference images, which are, respectively, recorded as UID-SIFCM, IR-SIFCM, CVA-SIFCM, and SDI-SIFCM (the proposed method). In the second group, PCA-K-means [36], FLICM [37], CWNN [38], and the proposed method are performed for comparative analysis in the second group of experiments. False alarms (FAs), missed alarms (MAs), overall accuracy (OA) [39], Kappa, and F-measure [40] are used as quantitative evaluation indexes to measure the quality of change detection results.

This method involves many parameters, $c = 2$ and $\pi_{ij}(x)$, which can be calculated by equation (7). The parameters that may affect the results of the proposed method are mainly $\varepsilon$ and *max_iter*. In order to verify the effect of $\varepsilon$ and *max_iter* on the experimental results, the values of $\varepsilon$ will be 0.03, 0.05, and 0.07; *max_iter* will be 50, 100, and 300, and Figures 2 and 3 will be used as experimental data. The actual number of iterations in Figures 2 and 3 is 18~19 and 28~29 times. Therefore, *max_iter* has a value of 50, 100, and 300, and the change detection accuracy is the same. Therefore, the number of iterations in this experiment is 50. At the same time, under the premise of determining *max_iter* = 50, the values of $\varepsilon$ are set as 0.03, 0.05, and 0.07. The accuracy does not change from different values, so here we choose $\varepsilon = 0.05$.

*3.2.1. Comparative Experimental Results Analysis of the First Group.* Figures 2(d)–2(g) are the change detection results of the first group of images through UID-SIFCM, IR-SIFCM, CVA-SIFCM, and SDI-SIFCM, respectively. Figures 3(d)–3(g) show the change detection results of the second group of images by UID-SIFCM, IR-SIFCM, CVA-SIFCM, and SDI-SIFCM, respectively. It can be seen from the comparison between Figures 2 and 3 that change detection results of the proposed method are better than results of the other three methods. From Figures 4 and 5 and Tables 1 and 2, the same conclusion can be drawn.

For two sets of images, the proposed method has the highest OA, Kappa, and F-measure values, which are significantly better than the other three methods. The IR-SIFCM is only lower than the proposed method of the OA evaluation index, but there is a serious MA. The MA for the second group of images is as high as 98.34%, and the Kappa and F-measure indicators of the second group of images are lowest; the results of UID-SIFCM and CVA-SIFCM are close to each other in the three evaluation indexes, and the

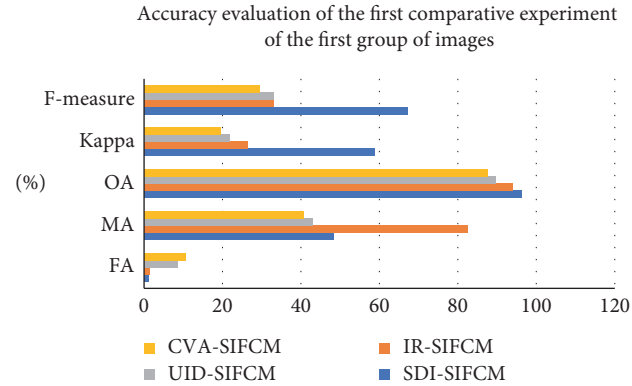


Figure 4: Bar graph of the first group of comparative experimental results of the first group of images.

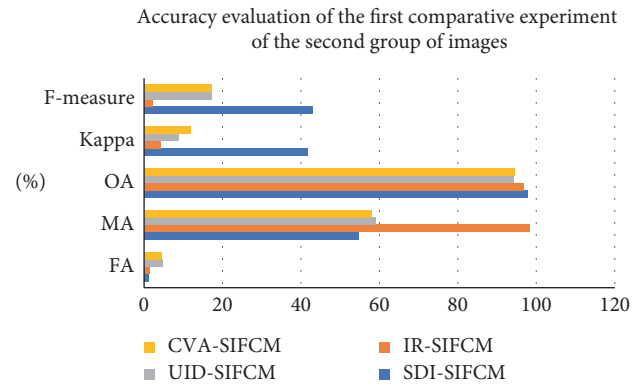


Figure 5: Bar graph of the first group of comparative experimental results of the second group of images.

obtained change detection results are also similar; the comprehensive performance is lower than the proposed method. From the visual comparison and quantitative evaluation, we can see that compared with the difference images constructed by the traditional UID, IR and CVA, the difference image constructed by the SDI has the highest quality. The experimental results verify the feasibility and reliability of the proposed method.

*3.2.2. Comparative Experimental Result Analysis of the Second Group.* Figures 2(g)–2(j) are the change detection results of the first group of images through the proposed method, PCA-K-means, FLICM, and CWNN, respectively. Figures 3(g)–3(j) show the change detection results of the second group of images by the proposed method, PCA-K-means, FLICM, and CWNN, respectively. By comparing the results of Figures 2(c) and 3(c) with the above results, we can see that the change detection results obtained by the proposed method are closer to the reference image. From Figures 6 and 7 and Tables 3 and 4, we know that comparing PCA-K-means, FLICM, and CWNN with the proposed method, the highest OA, Kappa, and F-measure are obtained; the CWNN has the lowest OA, Kappa, and F-measure indicators. The CWNN has better performance for SAR images, but it has poorer effects on optical images,

Table 1: Accuracy evaluation of the first comparative experiment of the first group of images.

| Methods | FA (%) | MA (%) | OA (%) | Kappa (%) | F-measure (%) |
|---|---|---|---|---|---|
| SDI-SIFCM | 1.1 | 48.34 | 96.17 | 58.77 | 67.30 |
| IR-SIFCM | 1.37 | 82.46 | 93.95 | 26.26 | 32.90 |
| UID-SIFCM | 8.46 | 43.05 | 89.54 | 21.84 | 32.90 |
| CVA-SIFCM | 10.56 | 40.60 | 87.71 | 19.47 | 29.50 |

Table 2: Accuracy evaluation of the first comparative experiment of the second group of images.

| Methods | FA (%) | MA (%) | OA (%) | Kappa (%) | F-measure (%) |
|---|---|---|---|---|---|
| SDI-SIFCM | 1.05 | 54.76 | 97.89 | 41.56 | 42.90 |
| IR-SIFCM | 1.48 | 98.34 | 96.61 | 4.30 | 2.10 |
| UID-SIFCM | 4.64 | 59.01 | 94.29 | 8.77 | 17.20 |
| CVA-SIFCM | 4.58 | 57.97 | 94.37 | 11.94 | 17.20 |

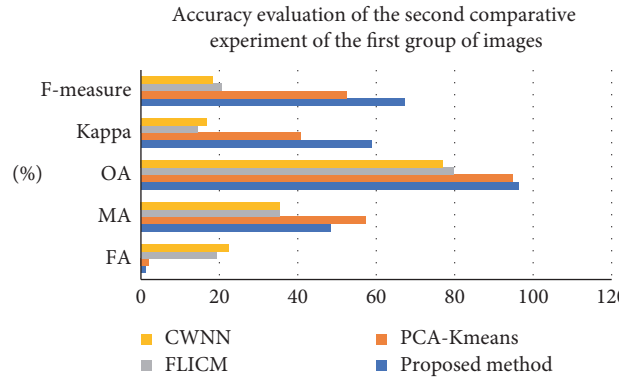


Figure 6: Bar graph of the second group of comparative experimental results of the first group of images.

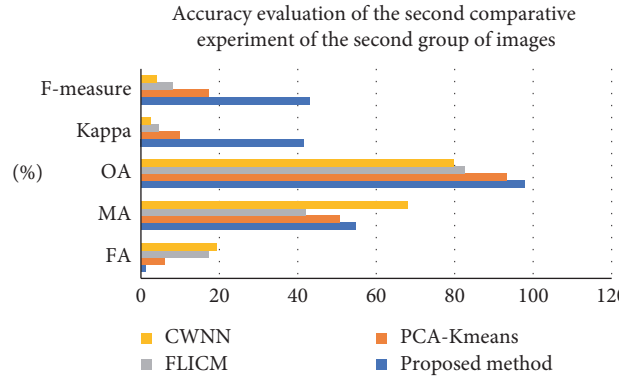


Figure 7: Bar graph of the second group of comparative experimental results of the second group of images.

Table 3: Accuracy evaluation of the second comparative experiment of the first group of images.

| Methods | FA (%) | MA (%) | OA (%) | Kappa (%) | F-measure (%) |
|---|---|---|---|---|---|
| Proposed method | 1.1 | 48.34 | 96.17 | 58.77 | 67.30 |
| PCA-K-means | 2.05 | 57.23 | 94.76 | 40.75 | 52.4 |
| FLICM | 19.3 | 35.38 | 79.77 | 14.56 | 20.50 |
| CWNN | 22.25 | 35.44 | 76.99 | 16.68 | 18.30 |

so further research is needed. PCA-K-means and FLICM are lower than the proposed method on the three indicators of OA, Kappa, and F-measure; Kappa and F-measure are significantly different from the proposed method. In the two sets of experiments, the accuracy of the four methods of the first group of images was higher than that of the second

Table 4: Accuracy evaluation of the second comparative experiment of the second group of images.

| Methods | FA (%) | MA (%) | OA (%) | Kappa (%) | F-measure (%) |
|---|---|---|---|---|---|
| Proposed method | 1.05 | 54.76 | 97.89 | 41.56 | 42.90 |
| PCA-K-means | 5.91 | 50.53 | 93.21 | 9.83 | 17.20 |
| FLICM | 17.11 | 42.00 | 82.40 | 4.61 | 8.00 |
| CWNN | 19.37 | 68.00 | 79.67 | 2.34 | 4.00 |

group. It can be seen from the visual comparison and quantitative evaluation that the proposed method has some advantages over the traditional method. The experimental results verify the effectiveness and reliability of the proposed method.

## 4. Conclusion

Direct comparison is a simple and effective change detection strategy for multitemporal remote-sensing images, but the quality of difference image directly affects the accuracy of subsequent change detection. Therefore, a difference image construction method based on saliency difference is proposed in this paper. First, the saliency images of two temporal remote-sensing images are obtained, respectively, and then the SDI is constructed by subtraction of the two saliency maps. In this paper, the SIFCM method is used in the difference image to obtain the change and unchange regions by two kinds of clustering. Two groups of multitemporal aerial remote-sensing images are selected as the experimental data, and the overall accuracy is 96.17% and 97.89%, respectively, which proves the validity and reliability of the proposed method. However, the proposed method highly depends on the saliency detection results, and if the detection effect of saliency is not good, it will directly affect the subsequent change detection accuracy. Therefore, how to obtain high-quality saliency detection results will be the focus of the next research.

## Data Availability

The data used to support the findings of this study are available from the corresponding author upon request.

## Conflicts of Interest

The authors declare that there are no conflicts of interest regarding the publication of this paper.

## Acknowledgments

This research work was supported by the National Natural Science Foundation of China (no. 41961039), the Applied Basic Research Programs of Science and Technology Department of Yunnan Province (no. 2018FB078), and the Key Laboratory of Surveying and Mapping Science and Geospatial Information Technology of Ministry of Natural Resources (no. 201911).

## References

[1] A. Novo-Fernández, S. Franks, C. Wehenkel, P. M. López-Serrano, M. Molinier, and C. A. López-Sánchez, "Landsat time series analysis for temperate forest cover change detection in the Sierra Madre Occidental, Durango, Mexico," *International Journal of Applied Earth Observation and Geoinformation*, vol. 73, no. 1, pp. 230–244, 2018.

[2] S. B. Chavan, C. S. Reddy, S. S. Rao, and K. K. Rao, "Assessing and predicting decadal forest cover changes and forest fragmentation in Kinnerasani wildlife sanctuary, Telangana, India," *Journal of the Indian Society of Remote Sensing*, vol. 46, no. 5, pp. 729–735, 2018.

[3] S. Le Hégarat-Mascle, C. Ottlé, and C. Guérin, "Land cover change detection at coarse spatial scales based on iterative estimation and previous state information," *Remote Sensing of Environment*, vol. 95, no. 4, pp. 464–479, 2005.

[4] Z. Lv, T. Liu, C. Shi, J. A. Benediktsson, and H. Du, "Novel land cover change detection method based on *K*-means clustering and adaptive majority voting using bitemporal remote sensing images," *IEEE Access*, vol. 7, pp. 34425–34437, 2019.

[5] F. Huang, L. Chen, K. Yin et al., "Object-oriented change detection and damage assessment using high-resolution remote sensing images, Tangjiao landslide, Three Gorges Reservoir, China," *Environmental Earth Sciences*, vol. 77, no. 5, p. 183, 2018.

[6] L. Wang, C. Li, Q. Ying et al., "China's urban expansion from 1990 to 2010 determined with satellite remote sensing," *Chinese Science Bulletin*, vol. 57, no. 22, pp. 2802–2812, 2012.

[7] Z. Zhang, F. Liu, X. Zhao et al., "Urban expansion in China based on remote sensing technology: a review," *Chinese Geographical Science*, vol. 28, no. 5, pp. 727–743, 2018.

[8] W. Q. Feng and Y. J. Zhang, "Object-oriented change detection for remote sensing images based on fuzzy comprehensive evaluation," *Geomatics and Information Science of Wuhan University*, vol. 41, no. 7, pp. 875–881, 2016.

[9] A. Singh, "Review article digital change detection techniques using remotely-sensed data," *International Journal of Remote Sensing*, vol. 10, no. 6, pp. 989–1003, 1989.

[10] Y. Bazi, L. Bruzzone, and F. Melgani, "An unsupervised approach based on the generalized Gaussian model to automatic change detection in multitemporal SAR images," *IEEE Transactions on Geoscience and Remote Sensing*, vol. 43, no. 4, pp. 874–887, 2005.

[11] M. Gong, Z. Zhou, and J. Ma, "Change detection in synthetic aperture radar images based on image fusion and fuzzy clustering," *IEEE Transactions on Image Processing*, vol. 21, no. 4, pp. 2141–2151, 2012.

[12] G. R. Ma, P. X. Li, and Q. Q. Qin, "Based on fusion and GGM change detection approach of remote sensing," *Journal of Remote Sensing*, vol. 11, no. 6, pp. 847–853, 2006.

[13] L. Huang, Y. Fang, X. Zuo, and X. Yu, "Automatic change detection method of multitemporal remote sensing images

based on 2D-OTSU algorithm improved by firefly algorithm," *Journal of Sensors*, vol. 2015, Article ID 327123, 8 pages, 2015.

[14] G. Gao, X. Wang, M. Niu et al., "Modified log-ratio operator for change detection of synthetic aperture radar targets in forest concealment," *Journal of Applied Remote Sensing*, vol. 8, no. 1, Article ID 083583, 2014.

[15] M.-L. Nordberg and J. Evertson, "Vegetation index differencing and linear regression for change detection in a Swedish mountain range using Landsat TM and ETM+ imagery," *Land Degradation & Development*, vol. 16, no. 2, pp. 139–149, 2005.

[16] M. Gong, Y. Yang, T. Zhan, X. Niu, and S. Li, "A generative discriminatory classified network for change detection in multispectral imagery," *IEEE Journal of Selected Topics in Applied Earth Observations and Remote Sensing*, vol. 12, no. 1, pp. 1–13, 2019.

[17] F. Bovolo and L. Bruzzone, "A theoretical framework for unsupervised change detection based on change vector analysis in the polar domain," *IEEE Transactions on Geoscience and Remote Sensing*, vol. 45, no. 1, pp. 218–236, 2007.

[18] L. P. Zhang and C. Wu, "Advance and future development of change detection for multi-temporal remote sensing imagery," *Acta Geodaetica et Cartographica Sinica*, vol. 46, no. 10, pp. 1447–1459, 2017.

[19] F. Bovolo, S. Marchesi, and L. Bruzzone, "A framework for automatic and unsupervised detection of multiple changes in multitemporal images," *IEEE Transactions on Geoscience and Remote Sensing*, vol. 50, no. 6, pp. 2196–2212, 2012.

[20] F. Thonfeld, H. Feilhauer, M. Braun, and G. Menz, "Robust change vector analysis (RCVA) for multi-sensor very high resolution optical satellite data," *International Journal of Applied Earth Observation and Geoinformation*, vol. 50, pp. 131–140, 2016.

[21] Y. Tang and L. Zhang, "Urban change analysis with multi-sensor multispectral imagery," *Remote Sensing*, vol. 9, no. 3, p. 252, 2017.

[22] L. Li, X. Li, Y. Zhang, L. Wang, and G. Ying, "Change detection for high-resolution remote sensing imagery using object-oriented change vector analysis method," in *Proceedings of the 2016 IEEE International Geoscience and Remote Sensing Symposium*, pp. 2873–2876, Beijing, China, July 2016.

[23] T. K. Jakka, Y. M. Reddy, and B. P. Rao, "GWDWT-FCM: change detection in SAR images using adaptive discrete wavelet transform with fuzzy C-mean clustering," *Journal of the Indian Society of Remote Sensing*, vol. 47, no. 3, pp. 379–390, 2019.

[24] U. H. Atasever, "A novel unsupervised change detection approach based on reconstruction independent component analysis and ABC-Kmeans clustering for environmental monitoring," *Environmental Monitoring and Assessment*, vol. 191, no. 7, p. 447, 2019.

[25] T. Celik, "A Bayesian approach to unsupervised multiscale change detection in synthetic aperture radar images," *Signal Processing*, vol. 90, no. 5, pp. 1471–1485, 2010.

[26] Z. Wu, Z. Hu, and Q. Fan, "Superpixel-based unsupervised change detection using multi-dimensional change vector analysis and SVM-based classification," *ISPRS Annals of Photogrammetry, Remote Sensing and Spatial Information Sciences*, vol. I-7, pp. 257–262, 2012.

[27] L. F. Wei, Z. W. Mou, X. Y. Wang et al., "Change detection of high resolution remote sensing image based on CRF model," *Bulletin of Surveying and Mapping*, vol. 9, pp. 28–31, 2017.

[28] A. Ghosh, N. S. Mishra, and S. Ghosh, "Fuzzy clustering algorithms for unsupervised change detection in remote sensing images," *Information Sciences*, vol. 181, no. 4, pp. 699–715, 2011.

[29] M.-M. Cheng, N. J. Mitra, X. Huang, P. H. S. Torr, and S.-M. Hu, "Global contrast based salient region detection," *IEEE Transactions on Pattern Analysis and Machine Intelligence*, vol. 37, no. 3, pp. 569–582, 2015.

[30] B. Hou, Y. Wang, and Q. Liu, "A saliency guided semi-supervised building change detection method for high resolution remote sensing images," *Sensors*, vol. 16, no. 9, p. 1377, 2016.

[31] Q. L. Guo and J. P. Zhang, "Change detection for high resolution remote sensing image based on co-saliency strategy," in *Proceedings of the 2019 International Workshop on the Analysis of Multitemporal Remote Sensing Images*, pp. 1–4, Shanghai, China, August 2019.

[32] H. Fu, X. Cao, and Z. Tu, "Cluster-based co-saliency detection," *IEEE Transactions on Image Processing*, vol. 22, no. 10, pp. 3766–3778, 2013.

[33] B. K. Tripathy, A. Basu, and S. Govel, "Image segmentation using spatial intuitionistic fuzzy C means clustering," in *Proceedings of the 2014 IEEE International Conference on Computational Intelligence and Computing Research*, pp. 1–5, Coimbatore, India, December 2015.

[34] C. Benedek and T. Sziranyi, "Change detection in optical aerial images by a multilayer conditional mixed Markov model," *IEEE Transactions on Geoscience and Remote Sensing*, vol. 47, no. 10, pp. 3416–3430, 2009.

[35] C. Benedek and T. Szirányi, "A mixed Markov model for change detection in aerial photos with large time differences," in *International Conference on Pattern Recognition (ICPR)*, pp. 8–11, Tampa, FL, USA, December 2008.

[36] T Celik, "Unsupervised change detection in satellite images using principal component analysis and *k*-means clustering," *IEEE Geoscience and Remote Sensing Letters*, vol. 6, no. 4, pp. 772–776, 2009.

[37] R. Liu, Z. H. Jia, X. Z. Qin et al., "A new SAR image change detection based on FLICM algorithm," *Laser Journal*, vol. 36, no. 11, pp. 28–31, 2015.

[38] F. Gao, X. Wang, Y. Gao, J. Dong, and S. Wang, "Sea ice change detection in SAR images based on convolutional-wavelet neural networks," *IEEE Geoscience and Remote Sensing Letters*, vol. 16, no. 8, pp. 1240–1244, 2019.

[39] F. Bovolo and L. Bruzzone, "A detail-preserving scale-driven approach to change detection in multitemporal SAR images," *IEEE Transactions on Geoscience and Remote Sensing*, vol. 43, no. 12, pp. 2963–2972, 2005.

[40] B. Du, L. Ru, C. Wu, and L. Zhang, "Unsupervised deep slow feature analysis for change detection in multi-temporal remote sensing images," *IEEE Transactions on Geoscience and Remote Sensing*, vol. 57, no. 12, pp. 9976–9992, 2019.